applied sciences

MDPI

Article

Methylparaben Adsorption onto Activated Carbon and Activated Olive Stones: Comparative Analysis of Efficiency, Equilibrium, Kinetics and Effect of Graphene-Based Nanomaterials Addition

Gerardo León [1,*], Asunción María Hidalgo [2], Antonio Martínez [1], María Amelia Guzmán [1] and Beatriz Miguel [1]

[1] Departamento de Ingeniería Química y Ambiental, Universidad Politécnica de Cartagena, Paseo Alfonso XIII, 30203 Cartagena, Spain; antonio_3393@hotmail.com (A.M.); maguzmanmv@gmail.com (M.A.G.); beatriz.miguel@upct.es (B.M.)
[2] Departamento de Ingeniería Química, Campus de Espinardo, Universidad de Murcia, 30100 Murcia, Spain; ahidalgo@um.es
* Correspondence: gerardo.leon@upct.es

Featured Application: The content of this paper allows a positive assessment of the possibilities of using activated olive stones as a substitute adsorbent for activated carbon in the elimination of organic pollutants.

Abstract: This paper describes a comparative study of the adsorption of methylparaben onto commercial activated carbon and olive stones activated by calcination at 300 °C and treatment with 1 M HCl. The influence of the initial concentration of methylparaben, adsorbent dose, stirring speed and pH on the adsorption capacity of methylparaben on both adsorbents was studied. To find out the isotherm model, the kinetic model and the mechanism that best describe the adsorption process on each adsorbent, the experimental equilibrium data were analyzed using six isotherm models (Langmuir, Freundlich, Elovich, Temkin, Jovanovic and Dubinin–Radushkevich), and the experimental kinetic data were analyzed using four kinetic models (pseudo-first order, pseudo-second order, Elovich and Avrami) and two mechanistic models (Weber–Morris and Boyd). For both adsorbents, the Langmuir model best describes the adsorption equilibrium, the kinetics of the process follow a pseudo-first-order model and boundary layer diffusion is the step that mainly controls the adsorption process. The adsorption capacity of methylparaben on activated carbon is about four times higher than that of activated olive stones. The addition of graphene oxide and reduced graphene oxide to both adsorbents increases their methylparaben adsorption capacity, to a greater extent in the case of graphene oxide, being that increase more important in activated carbon than in activated olive stones.

Keywords: adsorption; methylparaben; activated carbon; activated olive stones; equilibrium; kinetics; mechanism; graphene-based nanomaterials

Citation: León, G.; Hidalgo, A.M.; Martínez, A.; Guzmán, M.A.; Miguel, B. Methylparaben Adsorption onto Activated Carbon and Activated Olive Stones: Comparative Analysis of Efficiency, Equilibrium, Kinetics and Effect of Graphene-Based Nanomaterial Addition. *Appl. Sci.* **2023**, *13*, 9147. https://doi.org/10.3390/app13169147

Academic Editor: Antonio Miotello

Received: 21 July 2023
Revised: 8 August 2023
Accepted: 8 August 2023
Published: 10 August 2023

1. Introduction

During the last decades, there has been an important growth in the world population, which has generated a great industrial expansion and a considerable technological development that has led to an increase in the presence of substances in the environment that can cause harmful effects on living beings [1]. Among these substances are the so-called emerging pollutants or pollutants of emerging concern, substances that are not regulated or controlled by national or international environmental authorities, whose presence in the environment is not necessarily new but about which there is growing concern for their potential

effects on human health and ecosystems [2,3]. They include compounds as varied in nature as pharmaceuticals, lifestyle products, drugs of abuse, personal care products, steroids and hormones, industrial additives or flame retardants [4], and their presence has been detected in different aqueous media and in a wide variety of concentrations [5].

Among personal care products, parabens (p-hydroxybenzoic acid alkyl and aryl esters) are widely used as preservatives in the pharmaceutical, food and cosmetic industries due to their high antibacterial and antifungal activity, stability over a wide pH range and low price [5,6], although they have been linked to various health problems, mainly breast cancer and reproductive disorders [7].

Methylparaben (MPB) is the most widely used paraben in commercial applications and, consequently, is the most frequently detected one in surface waters, at levels ranging from ng/L to μg/L [8].

Different methods have been described to remove methylparaben from aqueous media, including biodegradation [8], advanced oxidation processes [9–11], adsorption [12,13], membrane processes [14–16], constructed wetland systems [17] and electrochemical and sonoelectrochemical processes [18,19].

Adsorption is a widely recognized method for the removal of all types of pollutants from aqueous solutions due to its simplicity, economy and efficiency [20,21].

Although activated carbon is the adsorbent traditionally used to remove pollutants from aqueous solutions due to its large pore surface (with a controllable pore size), wide variety of surface functional groups, high efficiency, high adsorption rate and easy regeneration [22,23], research on the possibilities of using adsorbents derived from agrifood wastes has increased significantly in recent years [24–26].

In this paper, a comparative study of the removal of methylparaben from its aqueous solutions by adsorption onto activated carbon and activated olive stones is carried out, analyzing comparatively the efficiency of both processes, the equilibrium and kinetics models that best describe each of them and the mechanism of the adsorption process, identifying, for each adsorbent, the rate-controlling step of the global adsorption process.

In addition, the first results obtained in the study of the effect that the addition of graphene-based nanomaterials (graphene oxide and reduced graphene oxide) to both adsorbents has on the removal efficiency of methylparaben are also described and analyzed.

2. Materials and Methods

2.1. Materials

Methylparaben (methyl 4-hydroxybenzoate, 99%) was supplied by Alfa Aesar, Kandel (Germany). Activated carbon Darco AC 4–12 (surface area 600–675 m^2/gm) was obtained from Sigma-Aldrich, Steinheim (Germany). Crushed raw olive stones (ranging in size from 1 to 4 mm) were supplied by the olive oil mill Valle de Ricote, Archena, Murcia (Spain), and 36% HCl was supplied by Panreac, Darmstadt (Germany). Graphene oxide (99%) and reduced graphene oxide (80% C) were obtained from Abalonyx (Oslo, Norway).

2.2. Methods

2.2.1. Adsorbents Preparation

Commercial activated carbon (AC) was repeatedly washed with distilled water to remove the carbon dust it contained until the washing water was completely transparent. Then, it was dried in an oven at 105 °C for 24 h and stored in a desiccator.

Crushed olive stones were washed with distilled water and dried at 60 °C in an oven. In order to increase their active surface area, remove soluble components (tannins, resins, reducing sugars and dyes) and generate oxygenated functional groups (carboxyl, phenol, ketone and lactone), the olive stones were subjected to an activation process consisting of calcination at 300 °C for 3 h in a closed muffle furnace and subsequent treatment with 1 M HCl at room temperature (25 ± 2 °C) for 8 h [27,28]. Finally, the activated olive stones (AOS) were filtered, washed thoroughly with distilled water, dried at 100 °C for 24 h and

stored in a desiccator. The surface area of the prepared activated olive stones was 479 m^2/g [27].

Graphene-based nanocomposite-modified adsorbents were prepared from suspensions of 0.1% GO and rGO in water, obtained by applying ultrasound for 30 min at 10 min intervals separated by 5 min in an ice bath to avoid heating. A total of 50 mL of these suspensions were added to 150 mg of the adsorbents and sonicated again in the same way. Once the process was finished, the adsorbents were separated by settling, washed several times with distilled water, dried in an oven for 24 h and stored in a desiccator.

2.2.2. Effect of Experimental Parameters on Adsorption Process

The effects of the initial methylparaben concentration (10–50 mg/L), adsorbent dose (AC, 0.01–0.05 g; AOS, 0.02–0.10 g), initial pH of the pollutant solution (3–11) and stirring rate (80–240 rpm) on the removal efficiency were studied by varying the parameter under study and keeping the other parameters constant.

Batch experiments were performed in 50 mL Erlenmeyer flasks containing 40 mL of MPB solution of selected concentrations and pH and the appropriate amount of sorbent. The flasks were shaken at the selected speed on a thermostated shaker (20 °C) for 24 h. At that time, 1 mL of sample was taken and 2 mL of 1 M NaOH was added (basic pH provides a higher intensity of the MPB absorption band), determining MPB concentration by UV-Vis spectrophotometry at 289 nm using an Agilent 8453 spectrophotometer (Agilent Technologies, Santa Clara, CA, USA) from the calibration curve (concentration range: 10–60 mg/L; $R^2 = 0.9997$). The results obtained showed a maximum deviation of 4%.

The typical experimental conditions were as follows: initial methylparaben concentration, 50 mg/L; absorbent dose, (AC, 20 mg; AOS, 60 mg); initial pH of methylparaben solution, 7.0; stirring rate, 240 rpm; temperature, 293 K.

2.2.3. Equilibrium and Kinetic Experiments

In the equilibrium and kinetic experiments, the adsorption studies were carried out by shaking 0.02 g of AC or 0.06 g of AOS with 40 mL of MPB solutions of different concentrations (10–50 mg/L) for 24 h (equilibrium time) at pH 7 in a rotary shaker (50 mL Erlenmeyer flasks) at 240 rpm and at 20 °C, taking samples at different predetermined times and determining MPB concentration as described in the previous section.

The amount of MPB loaded onto the adsorbents at equilibrium, q_e (mg/g), and at any time t, q_t (mg/g), was determined by the following equations:

$$q_e = \left(C_0 - C_e\right) \cdot \frac{V}{m} \quad (1)$$

$$q_t = \left(C_0 - C_t\right) \cdot \frac{V}{m} \quad (2)$$

where C_0, C_t and C_e were the initial, time t and equilibrium MPB concentrations in the solution (mg/L), respectively; V was the volume of the MPB solution (L); and m was the mass of the adsorbent (g).

The data obtained from these experiments were used to analyze their fit to the different isotherm, kinetic and adsorption mechanism models by determining the corresponding correlation coefficients.

2.2.4. Mathematical Models

Equilibrium Studies

An adsorption isotherm represents an equilibrium relationship at a given temperature between the amount of adsorbate in the liquid phase and that on the adsorbent surface. In this paper, we analyze the fit of the equilibrium experimental data of MPB adsorption onto AC and AOS to six adsorption isotherm models (Langmuir, Freundlich, Elovich, Temkin, Jovanovic and Dubinin–Radushkevich) to determine which model best describes those processes (Table 1).

Table 1. Adsorption equilibrium mathematical models.

Model	Linearized Equation	Plot	Model Parameters
Langmuir [29–31]	$\frac{C_e}{q_e} = \frac{C_e}{q_m} + \frac{1}{q_m \cdot K_L}$ $R_L = \frac{1}{1 + K_L \cdot C_0}$	C_e/q_e against C_e	q_m: maximum monolayer adsorption capacity (mg/g) K_L: Langmuir adsorption constant (L/mg)
Freundlich [32–34]	$\ln q_e = \frac{1}{n} \cdot \ln C_e + \ln K_F$	$\ln q_e$ against $\ln C_e$	K_F : constant related to the adsorption capability (mg/g)·(L/mg)$^{1/n}$ n: constant related to adsorption intensity
Elovich [35]	$\ln \frac{q_e}{C_e} = \ln(K_E \cdot q_{mE}) - \frac{q_e}{q_{mE}}$	$\ln(q_e/C_e)$ against q_e	q_{mE}: maximum Elovich adsorption capacity (mg/g) K_E: Elovich equilibrium constant (L/mg)
Temkin [36–38]	$q_e = B \cdot \ln A + B \cdot \ln C_e$	q_e against $\ln C_e$	A: adsorption equilibrium constant (L/mg) B: the Temkin constant (mg/g)
Jovanovic [39,40]	$\ln q_e = \ln q_m - K_J \cdot C_e$	$\ln q_e$ against C_e	q_m: maximum adsorption capacity (mg/g) K_J is the Jovanovic constant (L/mg)
Dubinin–Radushkevich [41,42]	$\ln q_e = \ln q_m - K \cdot \varepsilon^2$ $\varepsilon = RT\ln\left(1 + \frac{1}{C_e}\right)$ $E = (2 \cdot K)^{-1/2}$	$\ln q_e$ against ε^2	q_m: maximum adsorption capacity (mg/g) K: constant related to the sorption energy (mol^2/J^2) ε: adsorption potential (J/mol) E: mean free energy of adsorption

Kinetic Studies

Adsorption kinetics describes the rate of retention of an adsorbate in a fluid environment on the surface of the adsorbent, determining the time required to reach equilibrium.

Four kinetic models (Lagergren pseudo-first order, Ho pseudo-second order, Elovich and Avrami) were used to determine the one that best describes methylparaben adsorption onto activated carbon and activated olive stones (Table 2).

Table 2. Adsorption kinetics mathematical models.

Model	Linearized Equation	Plot	Model Parameters
Pseudo-first order [43,44]	$\ln(q_e - q_t) = \ln q_{eps1} - k_{ps1} \cdot t$	$\ln(q_e - q_t)$ against t	k_{sp1} : pseudo-first order adsorption rate constant (1/min) q_{eps1}: equilibrium adsorption capacity estimated by the model (mg/g)
Pseudo-second order [45,46]	$\frac{t}{q_t} = \frac{1}{k_{ps2} \cdot q_{eps2}^2} + \frac{t}{q_{eps2}}$	t/q_t against t	k_{ps2}: pseudo-second order adsorption rate constant (L/mol·min) q_{eps2}: equilibrium adsorption capacity estimated by the model (mg/g)

Elovich [47,48]	$q_t = \frac{\ln(\alpha \cdot \beta)}{\beta} + \frac{\ln t}{\beta}$	q_t against ln t	α: initial adsorption rate (mg/g·min) β: constant related to the number of available adsorption sites (g/mg)
Avrami [49,50]	$\ln\left[-\ln\left(1-q_t/q_e\right)\right] = \ln K_{av} + n_{av} \cdot \ln t$	ln[−ln(1 − q_t/q_e)] against ln t	K_{av}: Avrami's constant rate (min^{-1}) n_{av}: Avrami's order model.

Adsorption Mechanism

The above kinetic models are not able to identify the diffusion mechanisms and the rate-controlling step that affect the adsorption process. Any solid–liquid sorption process is characterized by the following two mass transfer processes:

1. The adsorbate molecules diffuse from the bulk solution to the external surface of the adsorbent (boundary layer diffusion);
2. The adsorbate molecules diffuse through the interior of the adsorbent particles (intraparticle diffusion).

Any one of them, or a combination of both [51], can control the rate of the adsorption process.

The Weber–Morris intraparticle diffusion model and the Boyd model are used to identify the rate-controlling step of the adsorption process (Table 3).

Table 3. Adsorption mechanism mathematical models.

Model	Linearized Equation	Plot	Model Parameters
Weber-Morris [52]	$q_t = k_{intp} \cdot t^{1/2} + C_i$	q_t against $t^{1/2}$	k_{intp}: intraparticle diffusion rate constant (mg/g·$h^{1/2}$) C_i: contribution of the boundary layer diffusion
Boyd [53]	$B \cdot t = -0.4977 - \ln\left(1 - \frac{q_t}{q_e}\right)$	B.t against t	

When pure intraparticle diffusion exists, the Weber–Morris representation shows a straight line passing through the origin. The presence of multilinearity in that representation means that a combination of both boundary layer diffusion and intraparticle diffusion controls the adsorption process.

If the latter occurs, the Boyd kinetic model is used to identify the rate-controlling step of the adsorption process. If the plot of B·t versus time shows a straight line passing through the origin, the adsorption process is mainly controlled by intraparticle diffusion; otherwise, it is mainly controlled by boundary layer diffusion.

3. Results and Discussion

3.1. Effect of Experimental Parameters

3.1.1. Effect of the Initial Methylparaben Concentration

Increasing the initial concentration of methylparaben from 10 to 50 mg/L results in a significant increase in the adsorption capacity values of both adsorbents, from 18.87 mg/g to 77.18 mg/g in the case of activated carbon and from 4.33 mg/g to 15.95 mg/g in the case of activated olive stones (Figure 1a). This increase must be a result of the increased driving force to overcome the resistance to methylparaben mass transfer between the aqueous and the solid phases, which enhances the interaction between the methylparaben and the adsorbents [54].

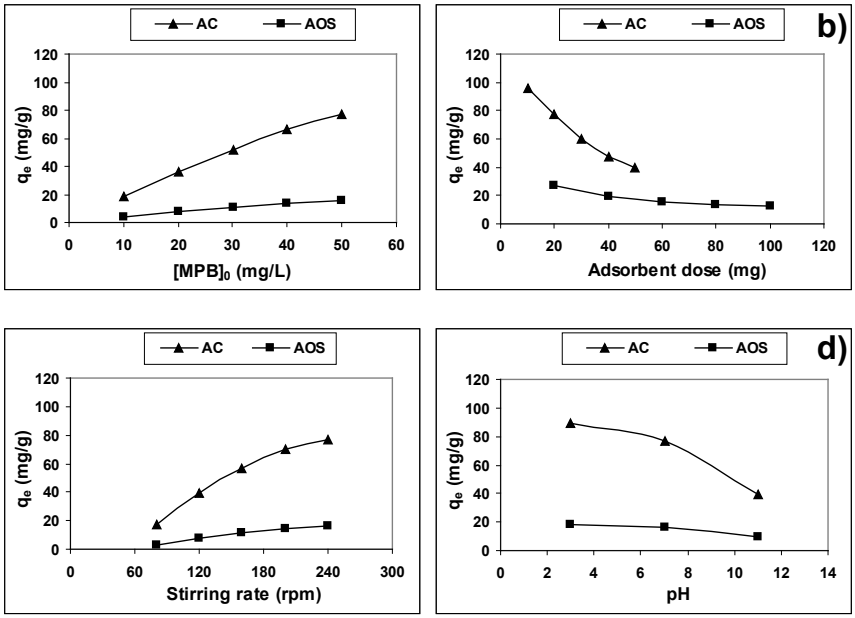

Figure 1. Effect of experimental parameters on the MPB adsorption onto AC and AOS (**a**): initial methylparaben concentration; (**b**) adsorbent dose; (**c**) stirring speed; (**d**) initial pH of methylparaben solution).

3.1.2. Effect of Adsorbent Dose

The amount of adsorbent used in the adsorption process gives the cost of the adsorbent per unit volume of the solution to be treated.

Increasing the adsorbent dose produces a decrease in the adsorption capacity values of both adsorbents (Figure 1b), from 95.58 to 39.73 (58.43% decrease) in the case of activated carbon (increase in dose from 10 mg to 50 mg) and from 27.23 to 12.25 (55.01% decrease) in the case of activated olive stones (increase in dose from 20 mg to 100 mg).

This decrease indicates that, in the adsorbent mass ranges used, although the mass of methylparaben adsorbed increases with the amount of adsorbent, as the total surface area available for adsorption (and, consequently, the total number of available adsorption sites) increases, the ratio of mass of methylparaben adsorbed per gram of adsorbent decreases as the initial concentration of methylparaben used remains unchanged [55].

For the same adsorbent dose (20 mg), the adsorption capacity of methylparaben on activated carbon (77.18 mg/g) is 4.05 times higher than its adsorption capacity on activated olive stones (19.07 mg/g) due to the greater surface area and the greater proportion of functional groups of the former with respect to the latter.

3.1.3. Effect of Stirring Speed

The effect of stirring speed on the removal of methylparaben by adsorption on activated carbon and activated olive stones is shown in Figure 1c. As can be seen, by increasing the stirring speed from 80 rpm to 240 rpm, the adsorption capacity of methylparaben increases from 17.26 mg/g to 77.18 mg/g (4.47 times) in the case of activated carbon and from 2.75 to 15.95 (5.80 times) in the case of activated olive stones. This increase is a consequence of the increased diffusion of methylparaben from inside the solution to the surface and inside the pores of the adsorbent.

3.1.4. Effect of the Initial pH of Methylparaben Solution

The pH of the adsorbate solution is a parameter that has a very important influence on the adsorption process by determining the ionization state of the functional groups and, consequently, the charge of both the adsorbate and the adsorbent. The effect of the

initial pH of the methylparaben solution on its adsorption on activated carbon and activated olive stones is shown in Figure 1d. It can be observed that the adsorption capacity of methylparaben on both adsorbents decreases with the increase in pH, with this decrease being more pronounced at basic pH values, especially in the case of activated carbon.

Methylparaben has a pKa value of 8.17 [7], which means that at values below this pH, it has no charge, and at higher values, it has a negative charge as a consequence of the ionization of the phenolic hydroxyl group.

The commercial activated carbon used has a zero charge point of 4.7 [56], which means that it will have a positive charge at pH values below 4.7 and a negative charge at higher pH values. Activated olive stones have a zero charge point of 3.5 [28], being positively charged at pH values below 3.5 and negatively charged at pH values above 3.5. With regard to the functional groups present on the surface of these adsorbents, the presence of carboxyl, phenol, anhydride, lactone, quinone and ether groups has been described in both activated carbon [57,58] and activated olive stones [28,59].

At pH 3, as methylparaben is in a neutral state and the two adsorbents are positively charged, some electrostatic interactions may occur between the positive zones of the adsorbents and the oxygens of the hydroxyl and ester groups of methylparaben (oxygens with a certain density of negative charge due to their inductive-I effect). This results in adsorption capacity values of 89.66 mg/g for activated carbon and 18.26 mg/g for activated olive stones.

At pH 7, methylparaben is in a neutral state and the two adsorbents are negatively charged, with the possibility of establishing hydrogen bridge interactions between the hydrogen of the hydroxyl group of the methylparaben and the negatively charged groups of the adsorbents, but with no possibility of the electrostatic interactions described in the previous paragraph. All this causes the adsorption capacity to decrease to values of 77.18 mg/g for AC (13.92% decrease) and 15.95 mg/g for AOS (12.65% decrease).

Finally, at pH 11, both methylparaben and the adsorbents are negatively charged, so there will be a significant electrostatic repulsion between the adsorbate and adsorbents, resulting in a significant decrease in the adsorption capacity of methylparaben, which decreases to values of 39.32 mg/g in AC (40.05% decrease in the value at pH 7 and 56.15% decrease in the value at pH 3) and of 10.03 mg/g in AOS (37.12% decrease in the value at pH 7 and 45.07% decrease in the value at pH 3).

3.1.5. Selected Standard Experimental Conditions

The selected standard experimental conditions were as follows: MPB initial concentration: 50 mg/L; adsorbent dose: 20 mg/L of AC and 60 mg/L of AOS; stirring speed: 240 rpm; initial methylparaben solution pH: 7.

3.2. Adsorption Equilibrium

In order to find out which isotherm model best describes the adsorption of methylparaben on activated carbon and activated olive stones, the experimental equilibrium data were fitted to the linearized mathematical equations of each of the six equilibrium models described above (Langmuir, Freundlich, Elovich, Temkin, Jovanovic and Dubinin–Radushkevich) by analyzing the correlation coefficients obtained in the corresponding linear regression.

Figures 2 and 3 show the linear representation of these six models for activated carbon and activated olive stones, respectively, while the values of their model constants and correlation coefficients (R^2) are included in Tables 4 and 5, respectively.

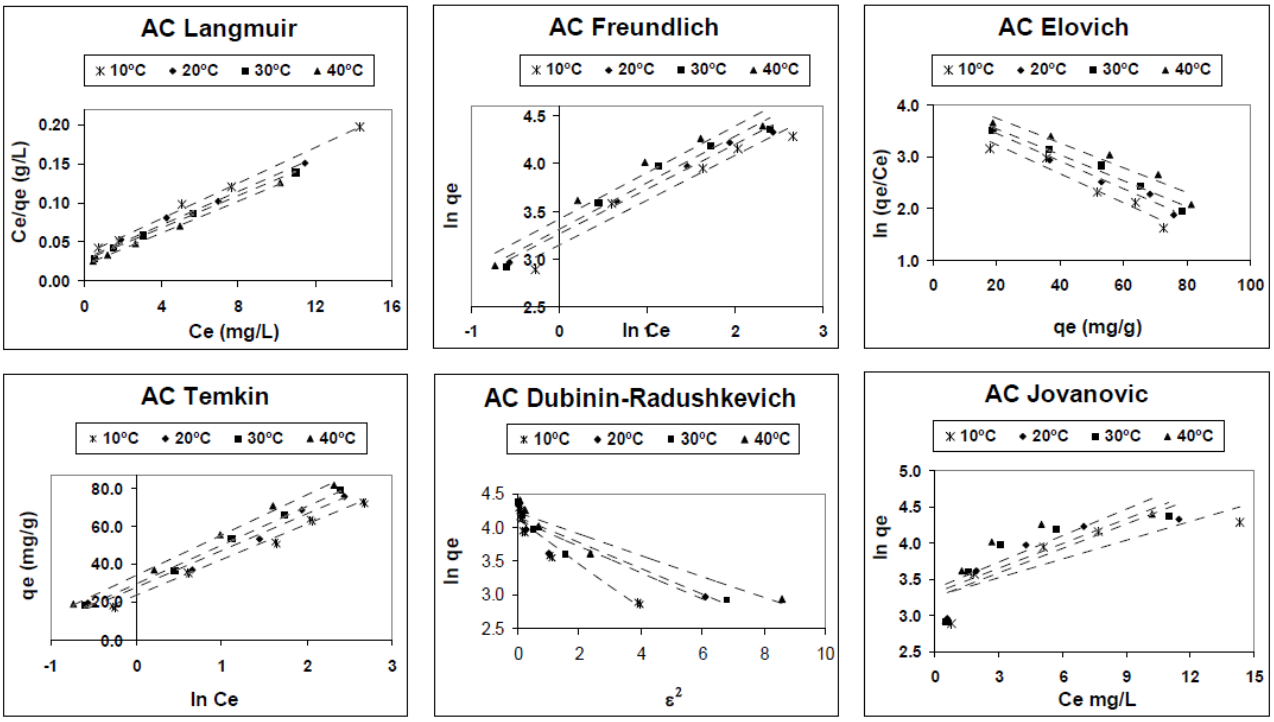

Figure 2. Isotherm plots for the adsorption of MPB onto AC.

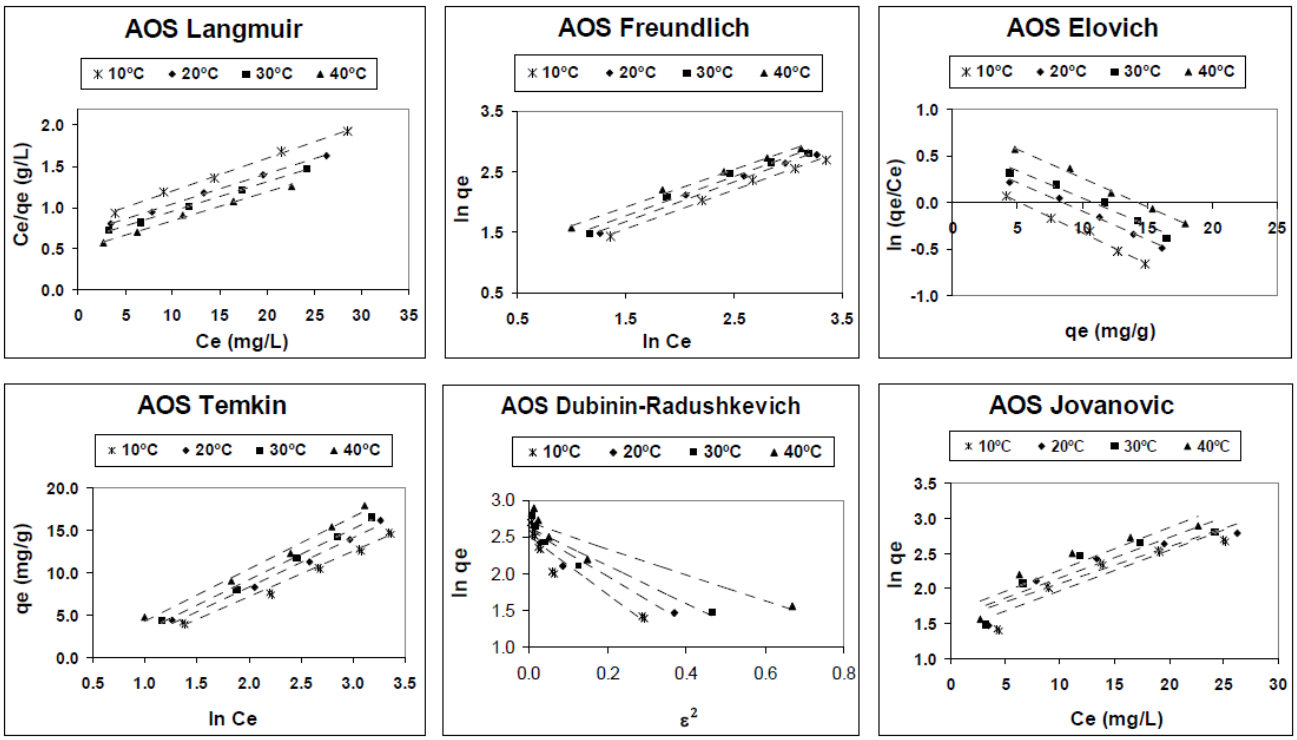

Figure 3. Isotherm plots for the adsorption of MPB onto AOS.

Table 4. Parameter values of the different studied isotherm models obtained in the adsorption of MPB onto AC.

	Langmuir Isotherm				Freundlich Isotherm			Elovich Isotherm		
Temperature (K)	q_m (mg/g)	K_L (L/mg)	R_L	R^2	n	K_F (mg/g)·(L/mg)$^{1/n}$	R^2	q_{mE} (mg/g)	K_E (L/g)	R^2
283	86.9565	0.3412	0.0554	0.9965	2.1277	23.2174	0.9561	35.7143	1.2451	0.9481
293	92.5926	0.3763	0.0505	0.9916	2.1418	26.1723	0.9901	36.7647	1.4985	0.9825
303	95.2381	0.4086	0.0467	0.9991	2.0509	27.3523	0.9687	39.8406	1.4412	0.9758
313	98.0392	0.4976	0.0386	0.9997	2.0631	30.5266	0.9537	41.6667	1.6557	0.9428
	Temkin isotherm			Jovanovic isotherm			Dubinin–Radushkevich isotherm			
Temperature (K)	A (L/mg)	B (mg/g)	R^2	q_m (mg/g)	K_J (L/mg)	R^2	q_m (mg/g)	K (mol^2/L^2)	E (Jmol)	R^2
283	3.5135	18.7006	0.9941	25.9378	0.0868	0.7008	61.2767	0.3284	1.2339	0.9305
293	4.1867	19.3489	0.9828	25.9352	0.1116	0.7689	61.3626	0.1978	1.5899	0.8620
303	4.2481	20.4452	0.9969	27.3086	0.1144	0.6915	63.5991	0.1904	1.6205	0.8993
313	5.0017	21.1908	0.9945	28.9595	0.1222	0.6542	68.1492	0.1581	1.7784	0.9211

Table 5. Parameter values of the different studied isotherm models obtained in the adsorption of MPB onto AOS.

	Langmuir Isotherm				Freundlich Isotherm			Elovich Isotherm		
Temperature (K)	q_m (mg/g)	K_L (L/mg)	R_L	R^2	N	K_F (mg/g)·(L/mg)$^{1/n}$	R^2	q_{mE} (mg/g)	K_E (L/g)	R^2
283	24.8756	0.0503	0.2846	0.9964	1.5601	1.8016	0.9923	14.8368	0.0958	0.9887
293	27.3224	0.0540	0.2701	0.9987	1.5413	2.0311	0.9903	16.4474	0.1015	0.9909
303	27.8552	0.0604	0.2487	0.9984	1.5309	2.2001	0.9852	16.1290	0.1495	0.9708
313	28.4900	0.0723	0.2167	0.9947	1.6116	2.6966	0.9920	17.1527	0.1092	0.9940
	Temkin isotherm			Jovanovic isotherm			Dubinin–Radushkevich isotherm			
Temperature (K)	A (L/mg)	B (mg/g)	R^2	q_m (mg/g)	K_J (L/mg)	R^2	q_m (mg/g)	K (mol^2/L^2)	E (Jmol)	R^2
283	1.9362	5.3355	0.9890	4.0020	0.0582	0.8876	12.4572	3.9969	0.3537	0.8882
293	1.7755	5.8183	0.9920	4.6409	0.0532	0.8649	13.6331	3.2111	0.3946	0.9019
303	1.6175	6.0015	0.9962	4.7870	0.0580	0.8475	13.8696	2.5785	0.4404	0.9222
313	1.3474	6.1344	0.9881	5.2169	0.0613	0.8644	14.8530	1.7796	0.5301	0.8911

The Langmuir isotherm best describes the adsorption process of methylparaben on both activated carbon and activated olive stones, showing the highest correlation coefficient values in all cases. The fit of the experimental data to the Langmuir isotherm model suggests that in the two adsorbents, the adsorption sites are homogeneously distributed and energetically equivalent, each adsorption site adsorbs only one methylparaben molecule and there is no interaction between the adsorbed methylparaben molecules. Moreover, the values of the R_L parameter are less than 1 in both adsorbents, indicating the favorable character of methylparaben adsorption on both activated carbon and activated olive stones [31].

The analysis of the Langmuir model constants for both adsorbents allows some significant conclusions to be drawn.

The maximum monolayer adsorption capacity (q_m) of methylparaben on activated carbon is 3.4 times higher than its value on activated olive stones, and the increase in temperature in both adsorbents indicates that the adsorption of methylparaben on both activated carbon and activated olive stones is endothermic.

The values of the Langmuir constant (K_L), related to the adsorbate–adsorbent affinity, allow us to affirm that the MPB/AC affinity is 6.85 times higher than the MPB/AOS affinity.

Although the Dubinin–Radushkevich model does not fit as well as the Langmuir model to the experimental data, the mean free energy of adsorption calculated from that model is less than eight in both adsorbents, suggesting the physical character of the adsorption process [42] and confirming the nature of the interactions described above in explaining the variations of adsorption with pH.

3.3. Adsorption Kinetics

As in the case of the isotherms, in order to determine the kinetic model that best describes the adsorption of methylparaben on activated carbon and activated olive stones, the experimental data on the variation of adsorption capacity with time were fitted to the linearized mathematical equations of the four kinetic models studied (Lagergren pseudo-first order, Ho pseudo-second order, Elovich and Avrami), and the correlation coefficients obtained were comparatively analyzed.

Linear representations of these four models for activated carbon and activated olive stones are shown in Figure 4, while the kinetic parameters and R^2 values calculated from these kinetic models are included in Tables 6 and 7.

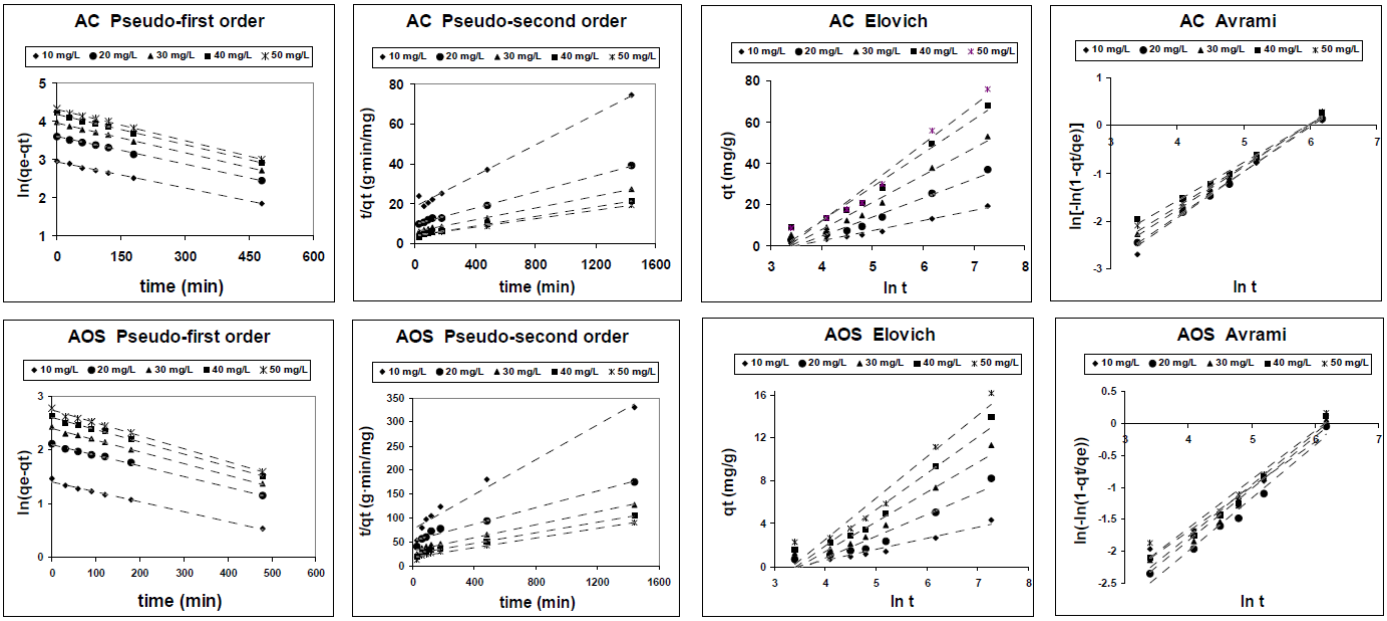

Figure 4. Kinetic plots for the adsorption of MPB onto AC and AOS.

These results allow us to state that while in the case of the activated olive stones, the experimental data clearly fit better to a pseudo-first-order kinetic model as the correlation coefficients obtained in this model are clearly higher than in the other three models, in the case of activated carbon, the values of the correlation coefficients of the pseudo-first and pseudo-second-order models are very similar, so it is not possible to establish a definitive conclusion. In order to discern which of these two models best defines the adsorption process of methylparaben on activated carbon, the greater/lesser coincidence of the experimental values of q_e with the values of this parameter obtained from pseudo-first and pseudo-second-order models was analyzed.

Table 6. Kinetic constants for the adsorption of MPB onto AC at 20 °C.

		Pseudo-First Order			Pseudo-Second Order			Elovich			Avrami		
Co (mg/L)	$q_{e,exp}$	k_{ps1} (1/min)	$q_{e,ps1}$ (mg/g)	R^2	k_{sp2} (g/mg·min)	$q_{e,ps2}$ (mg/g)	R^2	α (mg/g·min)	β (g/mg)	R^2	k_{AV} (1/min)	n_{AV}	R^2
10	19.3673	0.002284	18.7994	0.9956	0.00008153	25.8184	0.9899	0.1506	0.2081	0.9742	0.00288	0.9786	0.9854
20	36.9137	0.002395	36.3182	0.9981	0.00004340	49.0798	0.9979	0.2838	0.1083	0.9652	0.00346	0.9406	0.9978
30	53.1282	0.002578	51.8823	0.9990	0.00003762	67.6956	0.9984	0.4431	0.0762	0.9694	0.00462	0.9028	0.9986
40	68.2462	0.002653	65.2040	0.9973	0.00003767	83.0841	0.9946	0.6347	0.0613	0.9670	0.00821	0.8085	0.9905
50	75.7463	0.002720	74.3646	0.9986	0.00002845	95.2381	0.9932	0.6503	0.0537	0.9608	0.00584	0.8627	0.9880

Table 7. Kinetic constants for the adsorption of MPB onto AOS at 20 °C.

		Pseudo-First Order			Pseudo-Second Order			Elovich			Avrami		
Co (mg/L)	$q_{e,exp}$	k_{ps1} (1/min)	$q_{e,ps1}$ (mg/g)	R^2	k_{ps2} (g/mg·min)	$q_{e,ps2}$ (mg/g)	R^2	α (mg/g·min)	β (g/mg)	R^2	k_{AV} (1/min)	n_{AV}	R^2
10	5.9873	0.001861	4.1049	0.9904	0.00043281	5.5131	0.9714	0.0344	0.9907	0.9315	0.0112	0.7004	0.9800
20	10.6883	0.001953	8.1424	0.9960	0.00014076	11.6198	0.9668	0.0552	0.4960	0.9241	0.0048	0.8351	0.9771
30	14.3992	0.002161	11.0262	0.9979	0.00014026	14.9403	0.9810	0.0846	0.3637	0.9426	0.0060	0.8188	0.9749
40	18.7234	0.002265	13.5256	0.9979	0.00012871	17.9775	0.9856	0.1093	0.2966	0.9479	0.0066	0.8122	0.9808
50	18.7234	0.002381	15.5235	0.9960	0.00013105	20.2020	0.9821	0.1365	0.2606	0.9446	0.0093	0.7604	0.9590

Figure 5 shows this coincidence for both activated carbon and activated olive stones. It is observed that the theoretical qe values obtained by the pseudo-first-order model practically coincide with the experimental values of q_e; therefore, it can be concluded that the pseudo-first-order model is the one that best describes the adsorption of methylparaben on both activated carbon and activated olive stones.

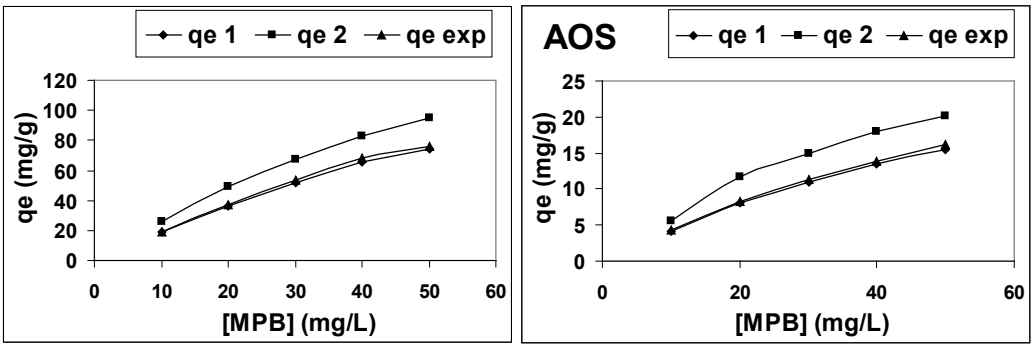

Figure 5. Experimental and theoretical values (from the pseudo-first and pseudo-second-order kinetic models) of the adsorption capacity of MPB onto AC and AOS at 20 °C.

The analysis of the model constants for both adsorbents shows that, in the adsorption of methylparaben on activated carbon, the pseudo-first-order rate constant and the equilibrium adsorption capacity calculated by the model are 1.19 and 4.68 times, respectively, higher than those obtained in the adsorption of methylparaben on activated olive stones, presumably because activated carbon has a larger surface area and a greater number of active sites (functional groups) than activated olive stones.

3.4. Adsorption Mechanism

In order to identify the mechanism of methylparaben adsorption onto activated carbon and activated olive stones, the kinetic experimental data were further analyzed by the Weber–Morris intraparticle diffusion and Boyd models.

As can be seen in Figure 6, the intraparticle model representations are not linear over the whole time range, with three distinct linear zones clearly distinguishable, which means that intraparticle diffusion is not the only controlling step of the adsorption rate,

with more than one controlling step involved. That is, the trial nature of the intraparticle model plots confirms that both boundary layer diffusion and intraparticle diffusion control the adsorption process in both adsorbents [60–62].

To distinguish the main rate-controlling step of the adsorption process, the experimental kinetic data were fitted to Boyd's kinetic model. Figure 6 shows that for both adsorbents, the plots are linear but do not pass through the origin, suggesting that the adsorption processes of methylparaben on both activated carbon and activated olive stones are mainly controlled by boundary layer diffusion [60–62].

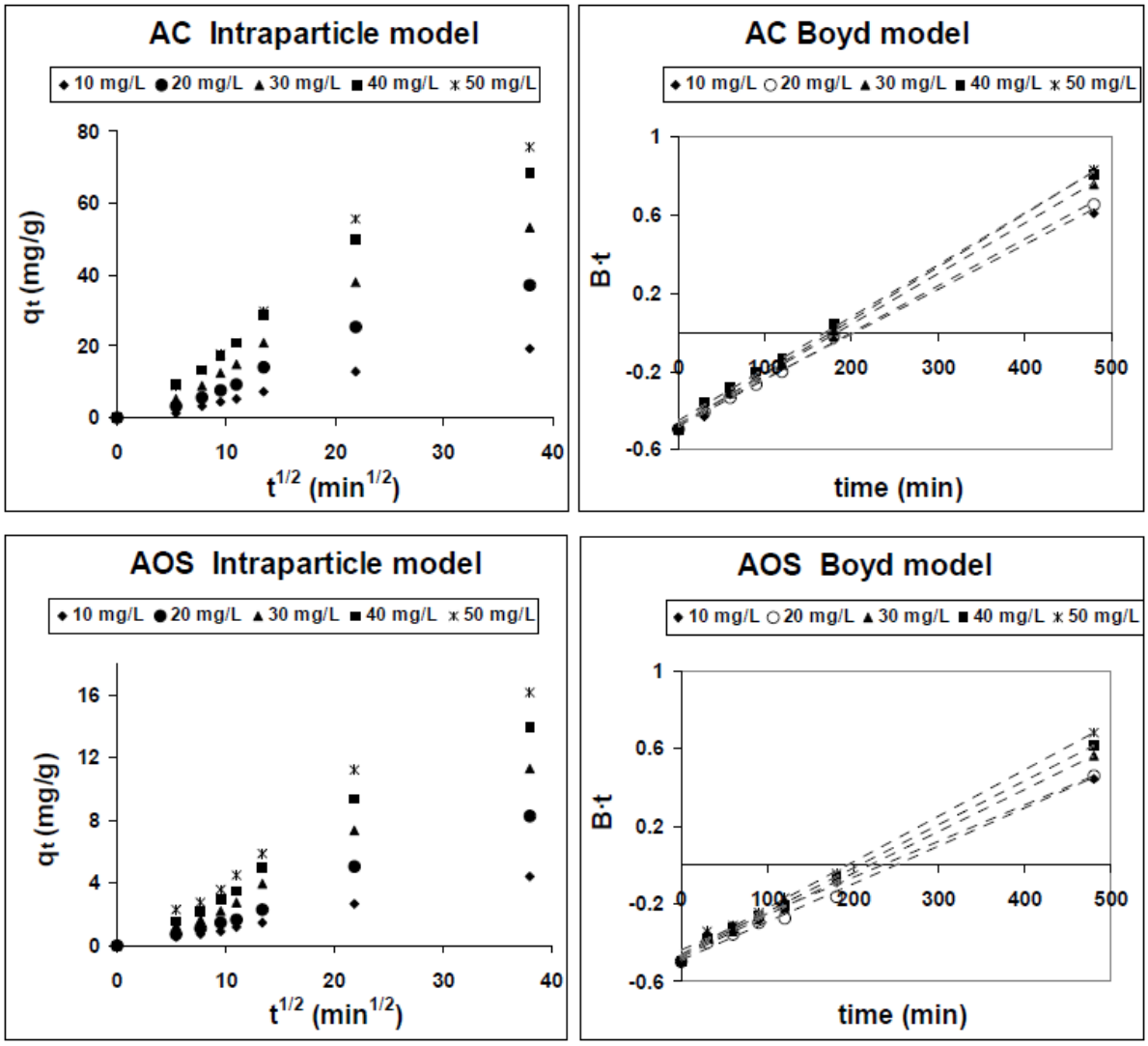

Figure 6. Adsorption mechanism plots for the adsorption of MPB onto AC and AOS.

3.5. Effect of the Presence of Graphene-Based Nanomaterials in Adsorbents on Methylparaben Adsorption

Modification of activated carbon and activated olive stones by the addition of graphene oxide or reduced graphene oxide leads to an increase in the adsorption capacity of methylparaben on both adsorbents (Figure 7).

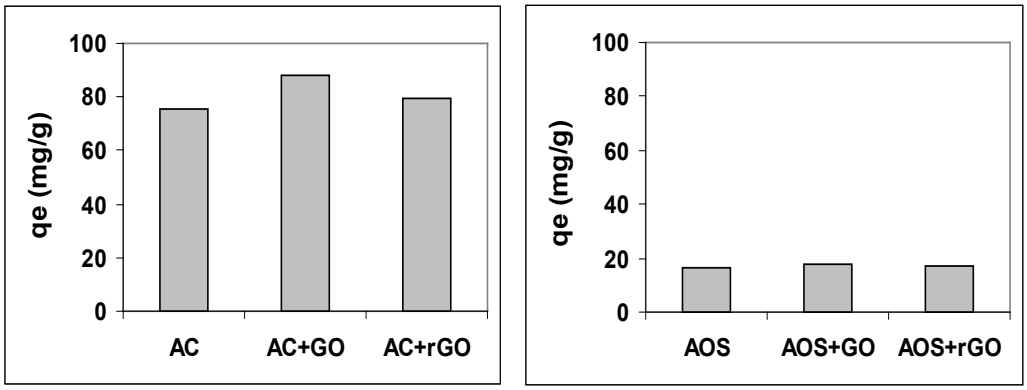

Figure 7. Effect GO and rGO presence in adsorbents on methylparaben adsorption (typical experimental conditions).

In the case of activated carbon, the addition of graphene oxide or reduced graphene oxide leads to increases in the methylparaben adsorption capacity of 16.6% and 5.1%, respectively, while in the case of activated olive stones, the increases are 11.8% and 4.0%, respectively. These increases must be the result of the modifications that the addition of GO and rGO produces in the surface characteristics of activated charcoal and activated olive stones [63].

On the one hand, graphene-based nanomaterials are characterized by their high porosity and high surface area [63], so their presence on the surface of the adsorbents under study should increase their surface area and adsorption capacity.

On the other hand, GO is the oxidized derivative of graphene that maintains the polyaromatic p-electron system of graphene and contains oxygenated polar functional groups, including hydroxyl, epoxide, carbonyl and carboxyl groups, with the carbonyl and carboxyl groups located at the edges and the epoxide and hydroxyl groups located in the basal plane of GO. Reduced graphene oxide (rGO), as a reduced form of GO, contains the same basic structure as GO but with fewer oxygenated polar functional groups. [64–66]. The additional contribution of oxygenated functional groups and polyaromatic p-electron systems that GO and rGO make to the surface of AC and AOS increases both the hydrogen bridge interactions (oxygenated functional groups of adsorbents/hydroxyl group of MPB) and the hydrophobic interactions (polyaromatic p-electron system of adsorbent/aromatic ring of MPB) between the adsorbents and MPB.

All this leads to the above-mentioned increase in the adsorption capacity of methylparaben by the modified adsorbents, which, for the reasons indicated, is higher in the modification with GO than with rGO. The greater increase in adsorption capacity observed in the CA with respect to the AOS must be a consequence of the greater amount of nanomaterial retained by the former due to its greater surface area.

4. Conclusions

A comparative study of the adsorption of methylparaben onto commercial activated carbon and olive stones activated by calcination at 300 °C and treatment with 1 M HCl was carried out in this paper. For both adsorbents, the methylparaben adsorption capacity increases with the increase in methylparaben concentration and stirring rate and decreases with the increase in adsorbent dose and pH.

At the same experimental conditions, the adsorption capacity of methylparaben onto activated carbon is about four times higher than that onto activated olive stones due to both higher surface area and higher MPB-AC adsorption interactions.

For both adsorbents, the methylparaben adsorption process is best described by the Langmuir isotherm model and the pseudo-first-order kinetic model, and it is mainly controlled by the boundary layer diffusion step. Langmuir model constants show that the

maximum monolayer adsorption capacity of MPB onto AC is 3.4 times higher than that onto AOS and that the MPB/AC affinity is 6.85 times higher than the MPB/AOS affinity.

Pseudo-first-order kinetic model constants show that MPB adsorption onto AC has an adsorption rate constant and a theoretical adsorption capacity of 1.19 and 4.68, respectively, times higher than MPB adsorption onto AOS.

The addition of graphene oxide and reduced graphene oxide to both adsorbents increases their methylparaben adsorption capacity due to modifications in the surface characteristics of the adsorbents related to the increase in both adsorption surface area as a consequence of the high porosity and high surface area of graphene nanomaterials and the number of functional groups that can interact with the methylparaben through hydrogen bridge interactions (oxygenated functional groups) and hydrophobic interactions (polyaromatic p-electron functional groups). These increases are more important in the case of graphene oxide, due to its higher oxygenated functional group presence, and in the case of activated carbon, due to its higher surface area and higher oxygenated functional group presence.

Author Contributions: Conceptualization, G.L., B.M. and A.M.H.; methodology, G.L., B.M. and A.M.H.; validation, G.L., A.M. and M.A.G.; formal analysis, G.L., A.M. and M.A.G.; investigation, G.L. and A.M.; resources, G.L. and B.M.; data curation, G.L., A.M. and M.A.G.; writing—original draft preparation, G.L. and M.A.G.; writing—review and editing, G.L., B.M. and A.M.H.; supervision, G.L. and B.M. All authors have read and agreed to the published version of the manuscript.

Funding: This research received no external funding.

Institutional Review Board Statement: Not applicable.

Informed Consent Statement: Not applicable.

Data Availability Statement: The data presented in this study are available on request from the corresponding author. The data are not publicly available due to they are part of a much larger study that is still underway.

Conflicts of Interest: The authors declare no conflict of interest.

References

1. Senthil-Rathi, B.; Senthil-Kumar, P.; Dai-Viet, N.V. Critical review on hazardous pollutants in water environment: Occurrence, monitoring, fate, removal technologies and risk assessment. *Sci. Total Environ.* **2021**, *797*, 149134.
2. Barceló, D. Emerging pollutants in water analysis. *Trends Anal. Chem.* **2003**, *22*, xiv–xvi.
3. Dulio, V.; Van Bavel, B.; Brorström-Lundén, E.; Harmsen, J.; Hollender, J.; Schlabach, M.; Slobodnik, J.; Thomas, K.; Koschorreck, J. Emerging pollutants in the EU: 10 years of NORMAN in support of environmental policies and regulations. *Environ. Sci. Eur.* **2018**, *30*, 5.
4. la Farré, M.; Pérez, S.; Kantiani, L.; Barceló, D. Fate and toxicity of emerging pollutants, their metabolites and transformation products in the aquatic environment. *Trends Anal. Chem.* **2008**, *27*, 991–1007.
5. Haman, C.; Dauchy, X.; Rosin, C.; Muñoz, J.F. Occurrence, fate and behavior of parabens in aquatic environments: A review. *Water Res.* **2015**, *68*, 1–11.
6. Gmurek, M.; Rossi, A.F.; Martins, R.C.; Quinta-Ferreira, R.M.; Ledakowicz, S. Photodegradation of single and mixture of parabens—Kinetic, by-products identification and cost-efficiency analysis. *Chem. Eng. J.* **2015**, *276*, 303–314.
7. Lincho, J.; Martins, R.C.; Gomes, J. Paraben Compounds—Part I: An Overview of Their Characteristics, Detection, and Impacts. *Appl. Sci.* **2021**, *11*, 2307.
8. Chang, X.; He, Y.; Song, L.; Ding, J.; Ren, S.; Lv, M.; Chen, L. Methylparaben toxicity and its removal by microalgae *Chlorella vulgaris* and *Phaeodactylum tricornutum*. *J. Hazard. Mater.* **2023**, *454*, 131528.
9. Sánchez-Martin, J.; Beltran-Heredia, J.; Dominguez, J.R. 2013. Advanced photochemical degradation of emerging pollutants: Methylparaben. *Water Air Soil. Pollut.* **2013**, *224*, 1483.
10. Lin, Y.; Ferronato, C.; Deng, N.; Wu, F.; Chovelon, J.M. Photocatalytic degradation of methylparaben by TiO_2: Multivariable experimental design and mechanism. *Appl. Catal. B–Environ.* **2009**, *88*, 32–41.
11. Zúñiga-Benítez, H.; Peñuela, G.A. Methylparaben removal using heterogeneous photocatalysis: Effect of operational parameters and mineralization/biodegradability studies. *Environ. Sci. Pollut. Res.* **2017**, *24*, 6022–6030.
12. Bernal-Romero, M.A.; Boluda-Botella, N.; Prats-Rico, D. Removal of emerging pollutants in water treatment plants: Adsorption of methyl and propylparaben onto powdered activated carbon. *Adsorption* **2019**, *25*, 983–999.

13. Bernal, V.; Giraldo, L.; Moreno-Piraján, J.C.; Balsamo, M.; Erto, A. Mechanisms of Methylparaben Adsorption onto Activated Carbons: Removal Tests Supported by a Calorimetric Study of the Adsorbent–Adsorbate Interactions. *Molecules* **2019**, *24*, 413.
14. Shirasangi, R.; Kohli, H.P.; Gupta, S.; Chakraborty, M. Separation of methylparaben by emulsion liquid membrane: Optimization, characterization, stability and multiple cycles studies. *Colloids Surf. A* **2020**, *597*, 124761.
15. Hidalgo, A.M.; León, G.; Murcia, M.D.; Gómez, M.; Gómez, E.; Gómez, J.L. Using Pressure-Driven Membrane Processes to Remove Emerging Pollutants from Aqueous Solutions. *Int. J. Environ. Res. Public Health* **2021**, *18*, 4036.
16. Heo, J.; Kwon, D.; Beirns, E.; Tan, G.Y.A.; Lee, P.H.; Kim, J. Superior methylparaben removal by anaerobic fluidized bed ceramic membrane bioreactor with PVDF tubular fluidized biocarrier: Reactor performance and microbial community. *J. Environ. Chem. Eng.* **2023**, *11*, 109153.
17. Mutar, Z.H.; Mohammed, A.A.; Al-Baldawi, I.A. Optimization of Acetaminophen and Methylparaben Removal within Subsurface Batch Constructed Wetland Systems. *J. Ecol. Eng.* **2022**, *23*, 228–239.
18. Steter, J.R.; Brillas, E.; Sirés, I. On the selection of the anode material for the electrochemical removal of methylparaben from different aqueous media. *Electrochim. Acta* **2016**, *222*, 1464–1474.
19. Steter, J.R.; Dionisio, D.; Lanza, M.R.V.; Motheo, A.J. Electrochemical and sonoelectrochemical processes applied to the degradation of the endocrine disruptor methyl paraben. *J. Appl. Electrochem.* **2014**, *44*, 1317–1325.
20. Chowdhury, S.; Mishra, R.; Saha, P.; Kushwaha, P. Adsorption thermodynamics, kinetics and isosteric heat of adsorption of malachite green onto chemically modified rice husk. *Desalination* **2011**, *265*, 159–168.
21. Crini, G.; Lichtfouse, E. Advantages and disadvantages of techniques used for wastewater treatment. *Environ. Chem. Lett.* **2019**, *17*, 145–155.
22. Mezohegyi, G.; van der Zee, F.P.; Font, J.; Fortuny, A.; Fabregat, A. Towards advanced aqueous dye removal processes: A short review on the versatile role of activated carbon, *J. Environ. Manag.* **2012**, *102*, 148–164.
23. Halim, A.A.; Aziz, H.A.; Johari, M.A.M.; Ariffin, K.S. Comparison study of ammonia and COD adsorption on zeolite, activated carbon and composite materials in landfill leachate treatment. *Desalination* **2010**, *262*, 31–35.
24. Bedia, J.; Peñas-Garzón, M.; Gómez-Avilés, A.; Rodriguez, J.J.; Belver, C. A Review on the Synthesis and Characterization of Biomass-Derived Carbons for Adsorption of Emerging Contaminants from Water. *C–J. Carbon Res.* **2018**, *4*, 63.
25. Chen, Y.; Shi, J.; Du, Q.; Zhang, H.; Cui, Y. Antibiotic removal by agricultural waste biochars with different forms of iron oxide. *RSC Adv.* **2019**, *9*, 14143.
26. Matei, E.; Râpă, M.; Predescu, A.M.; Turcanu, A.A.; Vidu, R.; Predescu, C.; Bobirica, C.; Bobirica, L.; Orbec, C. Valorization of Agri-Food Wastes as Sustainable Eco-Materials for Wastewater Treatment: Current State and New Perspectives. *Materials* **2021**, *14*, 4581.
27. El-Bakouri, H.; Usero, J.; Morillo, J.; Ouassini, A. Adsorptive features of acid-treated olive stones for drin pesticides: Equilibrium, kinetic and thermodynamic modeling studies. *Biores. Technol.* **2009**, *100*, 4147–4155.
28. León, G.; Saura, F.; Hidalgo, A.M.; Miguel, B. Activated olive stones as a low-cost and environmentally friendly adsorbent for removing cephalosporin C from aqueous solutions. *Int. J. Environ. Res. Public Health* **2021**, *18*, 4489.
29. Langmuir, I. The adsorption of gases on plane surfaces of glass, Mica and platinum. *J. Am. Chem. Soc.* **1918**, *40*, 1361–1403.
30. Wang, J.; Guo, X. Adsorption isotherm models: Classification, physical meaning, application and solving method. *Chemosphere* **2020**, *258*, 127279.
31. Weber, T.; Chakravorti, R. Pore and solid diffusion models for fixed-bed adsorbers. *AIChE J.* **1974**, *20*, 228–238.
32. Freundlich, H. Over the adsorption in solution. *J. Phys. Chem.* **1906**, *57*, 385–471.
33. Foo, K.Y.; Hameed, B.H. Insights into the modeling of adsorption isotherm systems. *Chem. Eng. J.* **2010**, *156*, 2–10.
34. Al-Ghouti, M.A.; Da'ana, D.A. Guidelines for the use and interpretation of adsorption isotherm models: A review. *J. Hazard. Mater.* **2020**, *393*, 122383.
35. Gök, Ö.; Özcan, A.; Erdem, B.; Özcan, A.S. Prediction of the kinetics, equilibrium and thermodynamic parameters of adsorption of copper(II) ions onto 8-hydroxy quinoline immobilized bentonite. *Coll. Surf. A: Physicochem. Eng. Aspects* **2008**, *317*, 174–185.
36. Temkin, M.; Pyzhev, V. Kinetics of Ammonia synthesis on promoted Iron catalysts. *Acta. Physicochim. URSS* **1940**, *12*, 327–356.
37. Rajahmundry, G.K.; Garlapati, C.; Kumar, P.S.; Alwi, R.S.; Vo, D.V.N. Statistical analysis of adsorption isotherm models and its appropriate selection. *Chemosphere* **2021**, *276*, 130176.
38. León, G.; García, F.; Miguel, B.; Bayo, J. Equilibrium, kinetics and thermodynamic studies of methyl orange removal by adsorption onto granular activated carbon. *Desal. Water Treat.* **2016**, *57*, 17104–17117.
39. Jovanovic, D.S. Physical adsorption of gases. I: Isotherms for monolayer and multilayer adsorption. *Kolloid-Z. Z. Polym.* **1969**, *235*, 1203–1213.
40. Saadi, R.; Saadi, Z.; Fazaeli, R.; Fard, N. Monolayer and multilayer adsorption isotherm models for sorption from aqueous media. *Korean J. Chem. Eng.* **2015**, *32*, 787–799.
41. Dubinin, M.M.; Radushkevich, L.V. The equation of the characteristic curve of the activated charcoal. *Proc. Acad. Sci. USSR Phys. Chem. Sect.* **1947**, *55*, 331–337.
42. Dubinin, M. The potential theory of adsorption of gases and vapors for adsorbents with energetically non-uniform surfaces. *Chem. Rev.* **1960**, *60*, 235–241.
43. Lagergren, S. About the theory of so-called adsorption of soluble substances. *K. Sven. Vetenskap. Handl.* **1898**, *24*, 1–39.
44. Tseng, R.L.; Wu, F.C.; Juang, R.S. Characteristics and applications of the Lagergren's first-order equation for adsorption kinetics. *J. Taiwan Inst. Chem. Eng.* **2010**, *41*, 661–669.

45. Ho, Y.S. Review of second-order model for adsorption systems. *J. Hazard. Mater.* **2006**, *136*, 681–689.
46. Hubbe, M.A.; Azizian, S.; Douven, S. Implications of apparent pseudo-second-order adsorption kinetics onto cellulosic materials: A review. *BioRes.* **2019**, *14*, 7582–7626.
47. Elovich, S.Y.; Larinov, O.G. Theory of adsorption from solutions of non-electrolytes on solid (I) equation adsorption from solutions and the analysis of its simplest form, (II) verification of the equation of adsorption isotherm from solutions. *Izv. Akad. Nauk. SSSR Otd. Khim. Nauk.* **1962**, *2*, 209–216.
48. Chien, S.H.; Clayton, W.R. Application of Elovich equation to the kinetics of phosphate release and sorption in soils. *Soil Sci. Soc. Am. J.* **1980**, *44*, 265–268.
49. Avrami, M. Kinetics of phase changes I General theory. *J. Chem. Phys.* **1940**, *7*, 1103–1112.
50. Vargas, A.M.M.; Cazetta, A.L.; Kunita, M.H.; Silva, T.L.; Almeida, V.C. Adsorption of methylene blue on activated carbon produced from flamboyant pods (*Delonix regia*): Study of adsorption isotherms and kinetic models. *Chem. Eng. J.* **2011**, *168*, 722–730.
51. Acharya, J.; Sahu, J.N.; Sahoo, B.K.; Mohanty, C.R.; Meikap, B.C. Removal of chromium(VI) from wastewater by activated carbon developed from Tamarind wood activated with zinc chloride. *Chem. Eng. J.* **2009**, *150*, 25–39.
52. Weber, W.J.; Morris, J.C. Kinetics of adsorption on carbon from solution. *ASCE Sanit. Eng. Div. J.* **1963**, *1*, 31–59.
53. Boyd, G.E.; Adamson, A.W.; Myers, L.S. The exchange adsorption of ions from aqueous solutions by organic zeolites. II. Kinetics. *J. Am. Chem. Soc.* **1947**, *69*, 2836–2848.
54. Kumar, P.S.; Ramakrishnan, K.; Kirupha, S.D.; Sivanesan, S. Thermodynamic, kinetic, and equilibrium studies on phenol removal by use of cashew nut shell. *Can. J. Chem. Eng.* **2011**, *89*, 284–291.
55. Lin, K.; Pan, J.; Chen, Y.; Cheng, R.; Xu, X. Study the adsorption of phenol from aqueous solution on hydroxyapatite nanopowders. *J. Hazard. Mater.* **2009**, *161*, 231–240.
56. Ahn, C.K.; Park, D.; Woo, S.H.; Park, J.M. Removal of cationic heavy metal from aqueous solution by activated carbon impregnated with anionic surfactants. *J. Hazard. Mater.* **2009**, *164*, 1130–1136.
57. Figueiredo, J.L.; Pereira, M.F.R.; Freitas, M.M.A.; Orfao, J.J.M. Modification of the surface chemistry of activated carbons. *Carbon* **1999**, *37*, 1379–1389.
58. Montes-Morán, M.A.; Suárez, D.; Menéndez, J.A.; Fuente, E. On the nature of basic sites on carbon surfaces: An overview. *Carbon* **2004**, *42*, 1219–1225.
59. Bohli, T.; Ouederni, A.; Fiol, N.; Villaescusa, I. Evaluation of an activated carbon from olive stones used as an adsorbent for heavy metal removal from aqueous phases. *Comptes Rendus Chim.* **2015**, *18*, 88–99.
60. Shahrin, E.W.E.S.; Narudin, N.A.K.; Shahri, N.N.M.; Verinda, S.B.; Nur, M.; Hobley, J.; Usman, A. Adsorption Behavior and Dynamic Interactions of Anionic Acid Blue 25 on Agricultural Waste. *Molecules* **2022**, *27*, 1718.
61. Asbollah, M.A.; Sahid, M.S.M.; Shahrin, E.W.E.S.; Narudin, N.A.K.; Kusrini, E.; Shahri, N.N.M.; Hobley, J.; Usman, A. Dynamics and thermodynamics for competitive adsorptive removal of methylene blue and rhodamine B from binary aqueous solution onto durian rind. *Environ. Monit. Assess.* **2022**, *194*, 645.
62. Shahrin, E.W.E.S.; Narudin, N.A.K.; Shahri, N.N.M.; Nur, M.; Lim, J.W.; Bilad, M.R.; Mahadi, A.H.; Hobley, J.; Usman, A. A comparative study of adsorption behavior of rifampicin, streptomycin, and ibuprofen contaminants from aqueous solutions onto chitosan: Dynamic interactions, kinetics, diffusions, and mechanisms. *Emerg. Contam.* **2023**, *9*, 100199.
63. Kumar, V.; Lee, Y.S.; Shin, J.W.; Kim, K.H.; Kukkar, D.; Tsangd, Y.F. Potential applications of graphene-based nanomaterials as adsorbent for removal of volatile organic compounds. *Environ. Int*. **2020**, *135*, 105356.
64. Faysal-Hossain, M.D.; Akther, N.; Zhou, Y. Recent advancements in graphene adsorbents for wastewater treatment: Current status and challenges. *Chin. Chem. Lett.* **2020**, *31*, 2525–2538.
65. Brisebois, P.P.; Siaj, M. Harvesting graphene oxide—Years 1859 to 2019: A review of its structure, synthesis, properties and exfoliation. *J. Mater. Chem. C* **2020**, *8*, 1517–1547.
66. Tadyszak, K.; Wychowaniec, J.K.; Litowczenko, J. Biomedical Applications of Graphene-Based Structures. *Nanomaterials* **2018**, *8*, 944.